

# Synthesis and Characterization of Carbon Nanotube–Polymer Multilayer Structures

Abha Misra,<sup>†</sup> Jordan R. Raney,<sup>‡</sup> Luigi De Nardo,<sup>§,⊥</sup> Anna E. Craig,<sup>‡</sup> and Chiara Daraio<sup>\*,\*</sup>

<sup>†</sup>Department of Instrumentation and Applied Physics, Indian Institute of Science, Bangalore, Karnataka, 560012, India, <sup>‡</sup>Division of Engineering and Applied Science, California Institute of Technology, Pasadena, California 91125, United States, <sup>§</sup>Istituto Nazionale di Scienza e Tecnologia dei Materiali, Milano, Italia, and <sup>⊥</sup>Dipartimento di Chimica, Materiali e Ingegneria Chimica “G. Natta”, Politecnico di Milano, Milano, Italy

In recent years, vertically aligned arrays of carbon nanotubes (CNTs) have been developed and considered for use as lightweight energy dispersive materials.<sup>1,2</sup> CNTs exhibit unique mechanical attributes similar to those found in fibrous materials,<sup>3</sup> having excellent compression capability coupled with extreme structural flexibility and recovery.<sup>4</sup> CNTs have the added benefit of presenting a high electrical conductivity, which can be exploited for the creation of multifunctional materials or for active strain monitoring in response to external mechanical loading.<sup>5</sup> The design and functionality of CNT-based structures has evolved and benefited from an understanding of non-linear stress wave mitigation and deformation mechanisms of cellular foams.<sup>6,7</sup>

A common protection scheme that is often adopted for impact mitigation and vibration damping is to utilize layered structures composed of materials with different acoustic impedance.<sup>8</sup> The approach has proven to be quite effective in the design of protective systems in which fiber-reinforced composites<sup>9</sup> or porous foam-like materials are combined with polymers and/or metals<sup>10</sup> to create highly efficient vibration and energy dampers. For practical applications, weight reduction plays an important role and requires the integration of new multifunctional materials based upon microstructural design. These characteristics suggest the use of CNT arrays as lightweight components in the assembly of protective devices against impacts and vibrations.

Preliminary investigations on the mechanical response of CNT arrays partially embedded in polymer have shown enhanced energy absorption capability and sensitivity to large differences in strain rate.<sup>6</sup> In addition, aligned arrays of CNTs grown *via* thermal chemical vapor deposition have

**ABSTRACT** We develop lightweight, multilayer materials composed of alternating layers of poly dimethyl siloxane (PDMS) polymer and vertically aligned carbon nanotube (CNT) arrays, and characterize their mechanical response in compression. The CNT arrays used in the assembly are synthesized with graded mechanical properties along their thickness, and their use enables the creation of multilayer structures with low density (0.12–0.28 g/cm<sup>3</sup>). We test the mechanical response of structures composed of different numbers of CNT layers partially embedded in PDMS polymer, under quasi-static and dynamic loading. The resulting materials exhibit a hierarchical, fibrous structure with unique mechanical properties: They can sustain large compressive deformations (up to ~0.8 strain) with a nearly complete recovery and present strain localization in selected sections of the materials. Energy absorption, as determined by the hysteresis observed in stress–strain curves, is found to be at least 3 orders of magnitude larger than that of natural and synthetic cellular materials of comparable density. Conductive bucky paper is included within the polymer interlayers. This allows the measurement of resistance variation as a function of applied stress, showing strong correlation with the observed strain localization in compression.

**KEYWORDS:** carbon nanotubes · multilayer · energy absorption · bucky paper · strain rate · bulk density

been reported to exhibit graded mechanical properties along their length and a foam-like behavior in compression.<sup>2</sup> The base of CNT arrays (*i.e.*, the side nearer the substrate during synthesis) is generally softer and more prone to buckling and deformation.<sup>2</sup> These properties make CNT arrays excellent candidates as energy-absorbing materials, in particular for dynamic applications.

Multilayer arrays of CNTs are expected to present yet improved protective properties. The synthesis of hybrid materials based on alternating CNT and vermiculite inorganic layers has been reported.<sup>11</sup> Similarly, a multilayer structure consisting of alternating layers of aligned CNTs and metal foils has been described.<sup>12</sup> In both cases, the weak adhesion between the CNT foams and the interlayers limits their protective performance. The present study is focused on the fabrication and characterization of multilayer structures

\* Address correspondence to daraio@caltech.edu.

Received for review June 20, 2011 and accepted September 23, 2011.

Published online September 25, 2011  
10.1021/nn202262j

© 2011 American Chemical Society

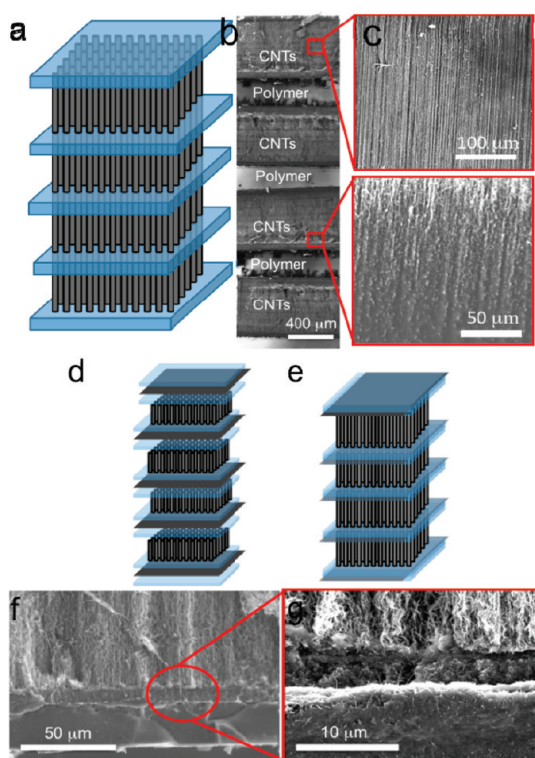


**Figure 1.** Multilayer carbon nanotube–polymer assembly. (a) Schematic diagram of the four-layer carbon nanotube–polymer (PDMS) structure. (b) Optical image of the four-layer carbon nanotube–polymer structure. (c) Scanning electron microscope (SEM) image showing the free-standing and wetted portions of the CNT array. (d) Schematic diagram of the assembly of a multilayered CNT system with embedded polymer–bucky paper layers. (e) Final arrangement of carbon nanotubes/polymer/bucky paper film. (f) SEM images showing the interface between the polymer with embedded bucky paper film and the CNTs. (g) Higher resolution image of the interface.

with compliant polymer interlayers, which show complete recovery after large compressive strain, without any damage at the interface between layers. The polymer layers reinforce the resilient aligned CNT bundles and act as an interface material to strengthen the multilayer structure. To evaluate the behavior of these layered structures, we performed mechanical tests with *in situ* electrical measurements and optical microscopy.

Vertically aligned arrays of carbon nanotubes were grown on thermally oxidized silicon by chemical vapor deposition using a one-stage thermal CVD system as described elsewhere.<sup>6</sup> A solution of ferrocene (catalyst) and toluene (carbon source) of 0.02 g mL<sup>-1</sup> was fed into the furnace, which was at a temperature of 825 °C throughout the process. The overall length of CNT bundles was measured to be  $\sim 800 \mu\text{m}$ . The CNT samples were taken off from the substrate using a razor blade, and the bulk density was determined by obtaining dimensions along the three axes and then dividing mass, as measured with a microbalance, by

the volume of the CNT block. This density has been measured to be 0.12–0.28 g cm<sup>-3</sup>.

After growth, a subset of samples was partially anchored in thin poly(dimethyl-siloxane) (PDMS) layers. The anchoring was obtained with a multistep process: first the PDMS was mixed with the curing agent in 10:1 ratio, and then the mixture was spin-coated on a glass slide at 700 rpm, to achieve a 50  $\mu\text{m}$  thick layer. This thickness was sufficient to connect two CNT bundles (as shown in schematic diagram Figure 1a) in a multilayer structure. The first layer of the CNT–polymer multilayer structure was created by embedding the end segments of the carbon nanotubes in a PDMS polymer layer *via* a substrate transfer method.<sup>6</sup> Figure 1a and b show that most of the CNT length is not embedded in the polymer. It was shown earlier that after curing the PDMS and CNT structure at 80 °C, the CNTs adhere well with the PDMS layer.<sup>13</sup> For the fabrication of the multilayer structure, the process was repeated sequentially for each layer in the structure. An image of the final multilayer structure, comprised of four CNT layers separated by polymer interlayers, is displayed in Figure 1b. The number of stacking layers can easily be extended utilizing the same fabrication process. The scanning electron microscope (SEM) images in Figure 1c and d show a close-up view of the polymer-free and embedded portions of the CNT array, respectively. This partial polymer embedding has structural and mechanical advantages in the layered structure: (1) it supports the CNT bases and tips, preventing separation between the layers during deformation, in contrast to what was observed in other reports,<sup>11</sup> and (2) it improves mechanical damping due to the compliant polymer matrix.<sup>3,14</sup>

A separate set of samples was prepared including a thin conducting film of entangled CNTs, commonly known as bucky paper (BP), within the polymer layers. The presence of this  $\sim 10 \mu\text{m}$  thick BP provided electrical continuity through each polymer layer and rendered the entire multilayer structure electrically conductive. The BP thin film was obtained by filtration of a CNT suspension in 2-propanol and water (25% vol). The films were individually sandwiched within PDMS layers, as shown by a schematic diagram in Figure 1d (the black layer shows the BP film, and PDMS layers are shown in a light color). The final multilayer CNT assembly is depicted in Figure 1e. A SEM image of the interface between the CNT and the polymer with BP is shown in Figure 1f, while a close-up view of the contact between the BP film in the polymer and the CNT arrays is shown in Figure 1g.

The quasi-static cyclic compressive response of the multilayer CNT–polymer assemblies was investigated using an Instron E3000. Compressive loads were applied along the CNT growth direction, as depicted in the inset schematic diagrams of Figure 2a. Displacement controlled compression tests were performed on single- and four-layer CNT assemblies partially

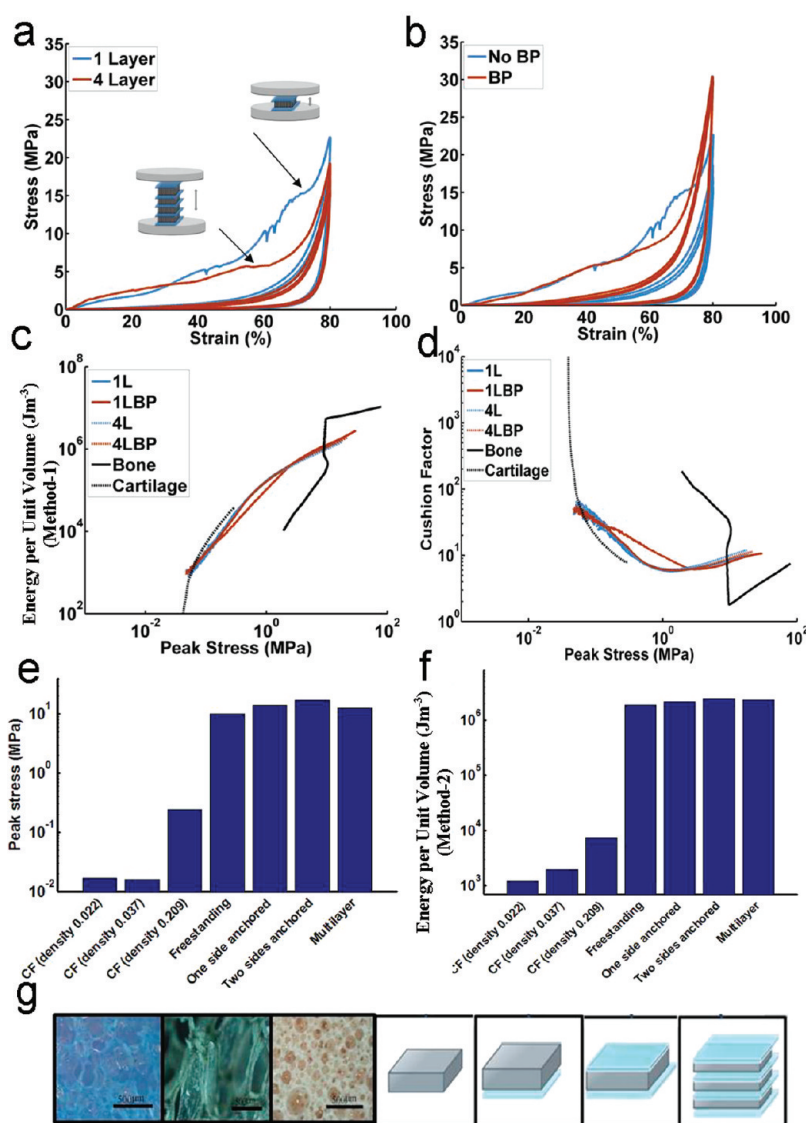


**Figure 2.** Quasi-static mechanical response and energy absorption. (a) Typical stress-strain curves obtained with single- and four-layer structures without insertion of bucky paper film. (b) Typical stress-strain curves obtained with single-layer structures with and without insertion of bucky paper films. (c) Energy absorption plots of single- and four-layer structures, calculated using method 1 and compared with cancellous bone and cartilage. (d) Cushion factor of single- and four-layer structures, compared with those of cartilage and bone. (e, f) Maximum peak stress and energy absorbed per unit volume, calculated using method 2, for commercial foams (CFs) and CNT structures. (g) Optical images of commercial foams with three different densities, 0.022, 0.037, and 0.209 g/cm<sup>3</sup> from left to right, respectively (scale bar is 500  $\mu$ m) and the schematic diagram of the CNT structures with and without polymer layer, from left to right, respectively.

embedded in PDMS layers. The goal of these mechanical investigations was to test the stability of the CNT–polymer interfaces and to characterize their ability to recover from large deformations. To ensure reproducibility of the results, measurements were acquired from six different samples for each type of structure (*i.e.*, a single CNT layer in PDMS, both with and without BP film, as well as CNT-PDMS structures with four CNT layers, with and without BP films). The stress–strain response was measured up to a set maximum compressive strain ( $\epsilon_{\text{max}} = 0.8$ ), determined so as to avoid reaching the maximum force capacity of the machine, and at two selected strain rates ( $10^{-2}$  and  $0.5 \text{ s}^{-1}$ ). We have not observed any strain rate dependence

on the compressive behavior of CNT bundles alone in this range of strain rates (*i.e.*,  $10^{-3}$  to  $0.5 \text{ s}^{-1}$ ), when the measured bulk density was accounted for (see Supporting Information).<sup>24</sup>

## RESULTS AND DISCUSSION

The representative stress–strain responses for three compressive cycles for single- and four-layer CNT structures, without BP films, are shown in Figure 2a. Figure 2b contains similar curves reporting the response of single-layer structures with and without BP films. Both single- and four-layer structures present a nonlinear loading–unloading path with a

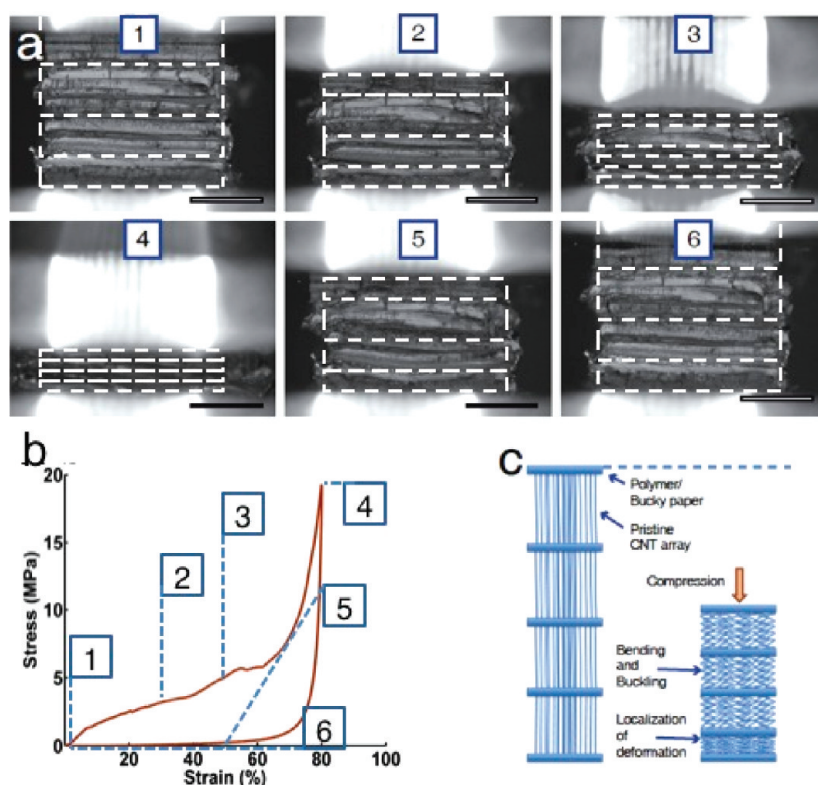


**Figure 3.** *In situ* visualization of the compressive deformation of a multilayer sample. (a) Digital snapshots of the deformed configuration of the four-layer structure corresponding to the different strain levels indicated in panel (b). The white lines show the position of polymer, which separates each CNT layer. (b) Stress–strain curve showing the different strain levels corresponding to the snapshots in panel (a). (c) Schematic diagram illustrating the localized deformation of the four-layer structure under compression.

hysteretic behavior in loading and unloading. This hysteresis was suggested to be a result of friction between the CNTs.<sup>2</sup> In all cases, a foam-like behavior is evident, similar to that already reported for free-standing vertically aligned CNT arrays.<sup>2,12</sup> The measured compressive stress–strain curves reveal three different regimes of deformation<sup>2,12,15</sup> characterized by (i) an initial linear elastic response at lower strains (less than 0.1), (ii) an intermediate region (between 0.1 and 0.6 strain) in which the deformation increases monotonically with small variation in the associated stress (a behavior characteristic of coordinated buckling and bending), and (iii) a final rise of the stress to a peak between 20 and 30 MPa (at the peak strain,  $\epsilon = 0.8$ ), resulting from densification and collapse of the overall assembly.<sup>11</sup>

To analyze the linear elastic response of the sample, we calculated low strain stiffness by a linear fitting of the initial linear elastic stress increase associated with the first loading cycle in the stress–strain curves (Figure 2a and b). We obtained the average value of this stiffness for the single-layer structure  $E = 9.9 \pm 1.8$  MPa and an enhanced modulus of  $16.3 \pm 1.9$  MPa for the four-layer structures in Figure 2a. However, samples including BP films resulted in a lower modulus for both the single- ( $9.1 \pm 1.7$  MPa) and four-layer ( $12.3 \pm 2.0$  MPa) structures.

The measured lower modulus is likely caused by the increase in thickness of the compliant polymer,<sup>16</sup> because structures with no BP have thinner polymer interlayers ( $\sim 50 \mu\text{m}$ ) than those with BP ( $\sim 100 \mu\text{m}$ ), and from the possible presence of slip between CNTs in the BP during compression.<sup>17</sup> Additional effects originating from the composite nature of the polymer/CNTs interface may contribute to the overall response of the samples, but have not been characterized as part of this study.

After the elastic region, the stress–strain response presented a monotonic increase in the stress between 0.1 and 0.6 strain. At strains higher than 0.6 the stress began to increase rapidly, reaching a maximum peak value of  $\sim 24$  MPa at the highest strain (0.8) for single-layer structures with no BP. Four-layer structures with no BP reached a maximum stress of 19 MPa (Figure 2a). Because of variation in  $L/D$  ratios (where  $L$  is the height and  $D$  is the lateral dimension of the area of the samples), the deformation mechanisms in compression may differ between samples. This implies that taller specimens might engage in compressive instabilities and non-uniaxial loading. In samples with BP films we observed higher peak stresses for both the single-layer ( $\sim 29$  MPa) (Figure 2b) and the four-layer structures ( $\sim 23$  MPa). The increase of the peak stress level in the structures with BP films can be

explained by an enhanced compressive strength due to the reinforcement of the carbon nanotube ends into polymer at the interfaces as compared to the cases of free-standing CNTs and polymer only as described in an earlier report.<sup>3</sup> According to this report,<sup>3</sup> the polymer around CNTs provides a confining effect, which results in strengthening of the composite interface in the structure.

The residual strain, which corresponds to the permanent deformation in the structure after compression, was observed to be about 0.05 in all samples. Both the peak stress and the hysteresis area were observed to decrease with an increasing number of compressive cycles. Figure 2a and b show the first three compressive cycles for each type of sample. There is little difference between the second and third compressive cycles for all samples shown, revealing that after only a couple cycles the majority of the compressive damage has taken place, with the material nearly in a steady-state response for further cycles. This is in agreement with earlier reports for free-standing CNT forests.<sup>2</sup> A similar characteristic behavior was also observed for multilayer structures with BP films.

The stress–strain curves obtained in the quasi-static tests (Figure 2a and b) were used to calculate the energy absorption capabilities of all samples. Depending on what material the CNT-based structures were being compared to, this quantity was calculated in two different ways. First, we show the energy absorbed during loading only (method 1), for comparison with materials having porous and layered microstructure that permanently deform in loading. Later, we calculate energy absorption as the area enclosed by the hysteresis loop between loading and unloading, to compare the response of our sample with protective materials that completely recover after loading (method 2). For the comparison with permanently deforming materials, we integrated the area under the loading portion of the stress–strain curves and plotted these values (per unit volume) up to a given peak stress as a function of the peak stress (Figure 2c). Although the CNT-based materials recover from strain, and therefore a portion of the energy absorption indicated for the CNT-based materials in these plots is a result of elastic energy that will be recovered, it is still useful to make the comparison of how the energy absorption capacity varies as a function of compression (peak stress) during loading. As observed in the stress–strain curves shown in Figure 2a and b the recovery or unloading portion of the hysteresis takes place at very low stress levels, meaning that the elastic strain energy recovered is a small portion of the total energy absorbed during loading. This allowed us to compare the energy absorption capabilities of our CNT–polymer-based materials with

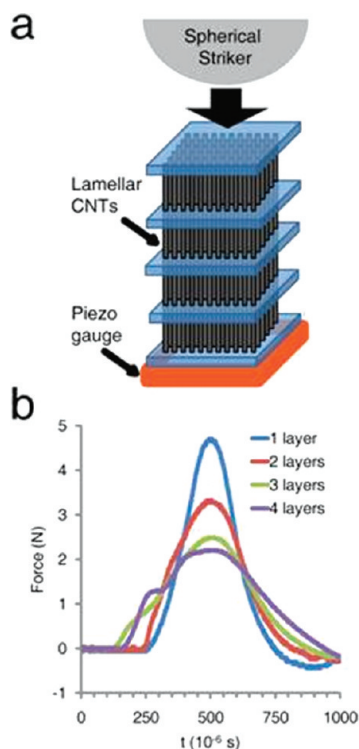


**Figure 4. Structure-dependent dynamic response. (a)** Schematic diagram showing the experimental setup. **(b)** Force–time plots obtained by impacting the CNT–polymer structures with a stainless steel bead at  $\sim 1.4 \text{ ms}^{-1}$ .

the energy absorption of biological materials that also employ a multilayer composite structure with a foam-like interior and a denser exterior region, such as cancellous bone<sup>18</sup> and lamellar fibers such as cartilage.<sup>19</sup> The data for biological materials were extracted from the reported stress–strain curves given in the references provided.<sup>18,19</sup> It is evident that the CNT-based materials have comparable or better energy adsorption capabilities than cartilage,<sup>19</sup> as a function of peak stress, despite having bulk densities between 0.12 and 0.28 g/cm<sup>3</sup> (as described above) compared to 1.12 g/cm<sup>3</sup> for cartilage.<sup>20</sup> Interestingly, the CNT-based materials also showed improved energy absorption over cancellous bone, up to a critical value of measured peak stress ( $\sim 10 \text{ MPa}$ ). At higher peak stresses, cancellous bone shows higher energy absorption than the CNT-based structures, most likely related to its larger density ( $\sim 1.85 \text{ g/cm}^3$ )<sup>21</sup> and more complex microstructure. We also calculated the cushion factor<sup>18</sup> as the measured peak stress over energy absorbed for the different CNT–polymer structures. The cushion factor values for all types of tested CNT–polymer structures were plotted against the peak stresses and compared with those for cartilage and bone (Figure 2d). In the lower peak stress regime, the cushion factor of CNT structures was found to be higher than the cartilage and bone structures. Among the CNT–polymer structures

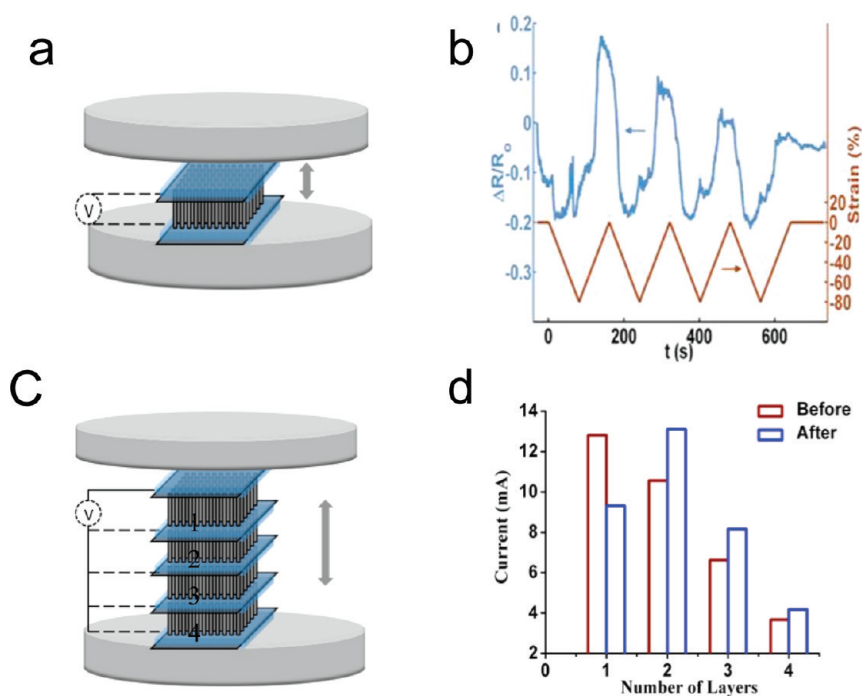


**Figure 5.** *In situ* and *ex situ* electrical response under applied stress. (a) The schematic diagram shows the experimental setup used for *in situ* cyclic compression on a single layer of CNT–polymer. (b) Compressive strain and fractional resistance change ( $\Delta R/R_0$ ) measured (*in situ*) during cyclic compression for an assembly of polymer, bucky paper, and a single layer of carbon nanotubes. (c) Schematic of the experimental setup used for electrical measurement of four-layer structure. (d) *Ex situ* electrical measurements performed after compressive testing of the multilayer samples. The graph shows the measured electric current before (red color) and after (blue color) compression of the four-layer structure. The dark line shows the constant position of one electrode, and dashed lines show the measurements between sequential layers with respect to the constant electrode.

both the energy absorption and cushion factors have not shown significant differences at any value of peak stress. The energy dissipation in our multilayer structures is expected to derive from frictional interactions between adjacent, entangled CNTs, in the section of the CNTs not embedded in polymer, and from the presence of a soft and compliant polymer interlayer partially embedding the CNTs. In addition, relative twisting of the CNT bundles may contribute to the energy dissipation, similar to what is observed in the shear interaction of CNT fibers.<sup>22,23</sup>

To evaluate the performance of our CNT–polymer structures in comparison with protective materials presenting large recovery after deformation, we selected different commercially available foams (CFs) obtained from microelectronic packaging and protective padding: cellulose fibers, polyurethane, and rubber. Densities of the CFs varied from 0.02 to 0.2 g cm<sup>-3</sup>. We compared the CNT-based structures to the CFs by comparing their quasi-static performance. The data are presented for tests performed at a strain rate of 0.05 s<sup>-1</sup>, though it should be noted that the response was found to be strain rate independent in this regime as discussed elsewhere.<sup>24</sup> We calculated the peak stress (Figure 2e) at maximum (0.8) strain. We also

compared energy absorption (Figure 2f). In this case we integrated the area of the hysteresis to account for both loading and unloading behavior, since both the CNT-based structures and the CFs recover from deformation. The CNT–polymer structures show a dramatic improvement of up to 3 orders of magnitude higher peak stress and energy absorption capability over CFs at comparable density. Optical microscopic images of the analyzed foam samples and the schematic diagram of CNT structures are depicted in Figure 2g.

For a detailed characterization of the deformation of multilayer structures, we coupled *in situ* optical measurements to the mechanical testing system. An optical microscope equipped with a digital camera allowed the real-time observation of the deformation of multilayer structures during compression and recovery, as a function of the applied compressive strain (see Figure 3a and b and the Supporting Information). A typical single-cycle compression test is reported in Figure 3 with snapshots acquired at different strains during testing. The dashed lines in Figure 3a are added to guide the eye for identifying the buckling and recovery response of the individual layers (the dashed lines indicate the location of the polymer interlayers).

Panel 1 in Figure 3a shows the pristine structure before compression (as indicated by point 1 in Figure 3b). The non-uniform gradual collapse of each layer at 30% strain (Figure 3b) is shown in panel 2 of Figure 3a. Upon reaching 50% strain, all layers have begun to collapse (panel 3 in Figure 3a, corresponding to point 3 in Figure 3b). This response demonstrates the presence of strain localization. At 0.8 strain, the layers show a homogeneous collapse (point 4). Points 5 and 6 show the nearly complete recovery of the structure as the strain returns to zero. A non-uniform recovery is shown in panel 5 of Figure 3c. The localized deformation and sequential buckling/recovery of the layers observed during testing is likely to be related to the graded stiffness in the microstructure and in the differences in CNT properties from one CNT layer to the next. Such variations have been shown to affect the mechanical properties of CNT arrays.<sup>24,25</sup> A schematic diagram explaining this phenomenon is shown in Figure 3c. This localized deformation of the individual layers is particularly relevant to the energy absorption of structures loaded dynamically.<sup>26</sup>

We assessed the dynamic response of the layered CNT–polymer structures by drop ball impact tests (see Methods section) (Figure 4a).<sup>27</sup> We evaluated the force mitigation performance of different CNT structures by comparing the peak force and length of contact time between samples composed of one, two, three, and four layers of CNTs under the same loading conditions (Figure 4b). The four-layer structure showed improved force mitigation capability as compared to the single-, double-, and triple-layer materials. In general, the peak force was observed to decrease with increasing number of layers, while at the same time, the contact duration increased. The onset of the deformation in the different layers of the multilayer structure is visible from the presence of “shoulders” in the force–time response, likely indicating the sequential collapse of individual layers and the localization of deformation within selected sections of the material.

The deformation of the CNT arrays and the effects of residual strain after cyclic compression were monitored *via in situ* and *ex situ* measurements (see Methods section) of electrical resistance across each layer of the CNT–polymer structures (Figure 5), assuming a constant contact resistance. The measurement of electrical resistance (Figure 5a) during cyclic tests revealed that materials composed of a single layer of CNTs present a decrease in electrical resistance (*in situ*) during loading, and an increase with unloading (Figure 5b). The observed variation in electrical resistance may be related to the structural reorganization of the individual CNTs within the array. It has been suggested that this reorganization results in an overlap of the electron states in adjacent CNT walls, leading to an increase in the

accessible number of electrical conduction channels while loading.<sup>28</sup> The distance between adjacent CNTs decreases when the CNTs bend in compression.<sup>28</sup> This may also increase the number of point contacts between CNTs and lower the resistance of the CNT arrays. The variation of resistance, defined as  $\Delta R/R_0$ , where  $\Delta R$  is the resistance change between the final and the pristine ( $R_0$ ) cases, was observed to decrease gradually after each cycle. Interestingly, we also noticed a permanent decrease of the electrical resistance after the load was completely removed, and this decrease can be attributed to the irreversible structural changes occurring in the CNT array structures.

*Ex situ* electrical measurements were performed on four-layer CNT structures. For this measurement the voltage was fixed at 5 V and the current was measured across each layer before and after the mechanical tests. Measurements were taken between the top layer (fixed electrode) and the successive layers (moving the electrode progressively from one layer to the next), as shown in the schematic diagram (Figure 5c). The electrical measurements acquired after performing the mechanical tests showed a significant difference as compared to the measurements acquired from the pristine sample. In particular, the current measured was different in each layer of the structure (Figure 5d). This suggests that the individual layers deform differently from one another and undergo different structural rearrangements. In this particular case, the current measured across the first layer was observed to decrease, as opposed to the increase measured across the other layers. This suggests a localization of deformation in the first layer of the structure, in agreement with the optical image shown in Figure 3a (panel 6). This effect may arise from the presence of imperfections deriving from the fabrication process.

## CONCLUSIONS

We report the design, fabrication, and testing of new lightweight multilayer materials for energy absorption, using structures composed of alternating layers of aligned carbon nanotubes and polymer (PDMS). The final materials combine a fibrous microstructure with graded mechanical properties. The presence of polymer interlayers provides adhesion and prevents delamination between different layers under mechanical loading. These materials have good energy-absorbing ability (up to 3 orders of magnitude better than conventional packaging foams of similar density) and present localized deformation within the individual layers composing the structure. The additional ability to include conducting bucky paper within the polymer interlayers provides electrical conductivity across the material's thickness without degradation of the overall

mechanical properties. *Ex situ* and *in situ* electrical and optical measurements have been performed,

revealing strain localization and differential collapse of the individual layers under compression.

## METHODS

**Dynamic Mechanical Characterization.** The experimental setup for high strain rate dynamic tests ( $\sim 10^3 \text{ s}^{-1}$ ) used a free-falling sphere (4.76 mm diameter, 0.45 g, Bearing-Quality Aircraft-Grade 25, Alloy Chrome Steel precision stainless steel ball, with a surface roughness  $\sim 50 \text{ nm}$  maximum, made from AISI type 52100 steel, McMaster-Carr) as a striker to impact the CNT samples. A calibrated piezosensor (Piezoelectric single sheet, T110-A4-602 provided by Piezo-System, Inc. with soldered 34 AWG microminiature wiring) connected to a Tektronix oscilloscope (TDS 2024B) was used to detect force–time curves under the sample. The impact was generated by dropping the steel sphere from a height of 10 cm, which corresponds to an impact speed of  $\sim 1.4 \text{ m s}^{-1}$ .

**Electrical Measurements.** Two-point electrical measurements were performed using an Alessi REL-3200 probe station attached to a Keithley-2365 source measure unit system. Bucky paper films were used as conducting electrodes to measure the changes in normalized electrical resistance during the compression of single layer (*in situ*)<sup>29</sup> and electrical current after recovery of the multilayer structures (*ex situ*). These measurements were monitored to observe changes due to the compression and recovery of the individual layers in both multi- and single-layer samples, similarly to the cyclic tests described in ref 29, for the measurement of resistance as a function of strain. The electrical current in the direction of the CNT growth was evaluated at a constant voltage of 5 V.

**Acknowledgment.** We thank H. M. (Chinthaka) Mallikarachi and S. Lacheteau for their contribution to the experiments. J.R.R. gratefully acknowledges support through a National Defense Science & Engineering Graduate (NDSEG) fellowship through the Department of Defense. L.D.N. thanks INSTM for travel granting support in “Metamateriali” grant project. C.D. acknowledges support from the Institute for Collaborative Biotechnologies under contract W911NF-09-D-0001 with the Army research office.

**Supporting Information Available:** *In situ* optical images were acquired during mechanical loading of the samples. An optical microscope was equipped with a digital camera to allow observation of the compressive deformation and recovery of the material as a function of the applied compressive strain (shown in the inset). Strain rate dependent mechanical response of as-grown carbon nanotubes is shown (S1). This material is available free of charge *via* the Internet at <http://pubs.acs.org>.

## REFERENCES AND NOTES

- Mylvaganam, K.; Zhang, L. C. Energy Absorption Capacity of Carbon Nanotubes Under Ballistic Impact. *Appl. Phys. Lett.* **2006**, *89*, 123127–123130.
- Cao, A.; Dickrell, P. L.; Sawyer, W. G.; Ghasemi-Nejhad, M. N.; Ajayan, P. M. Super-Compressible Foam Like Carbon Nanotube Films. *Science* **2005**, *310*, 1307–1310.
- Ci, L.; Suhr, J.; Pushparaj, V.; Zhang, X.; Ajayan, P. M. Continuous Carbon Nanotube Reinforced Composites. *Nano Lett.* **2008**, *8*, 2762–2766.
- Iijima, S.; Brabec, C.; Maiti, A.; Bernholc, J. Structural Flexibility of Carbon Nanotubes. *J. Chem. Phys.* **1996**, *104*, 2089–2092.
- Baughman, R. H.; Cui, C.; Zakhidov, A. A.; Iqbal, Z.; Barisci, J. N.; Spinks, G. M.; Wallace, G. G.; Mazzoldi, A.; De Rossi, D.; Rinzler, A. G.; *et al.* Carbon Nanotube Actuators. *Science* **1999**, *284*, 1340–1344.
- Misra, A.; Greer, J. R.; Daraio, C. Strain Rate Effects in the Mechanical Response of Polymer-Anchored Carbon Nanotube Foams. *Adv. Mater.* **2009**, *21*, 334–338.
- Ramachandra, S.; Kumar, P. Sudheer; Ramamurty, U. Impact Energy Absorption in an Al Foam at Low Velocities. *Scr. Mater.* **2003**, *49*, 741–745.
- Han, C.; Sun, C. T. Attenuation of Stress Wave Propagation in Periodically Layered Elastic Media. *J. Sound Vib.* **2001**, *243*, 747–761.
- Kireitseu, M. V. Vibration Damping Properties of Nanotube-Reinforced Materials. *Adv. Sci. Technol.* **2006**, *50*, 31–36.
- Kireitseu, M. V.; Bochkareva, L. Damping Properties of Sandwich Metal-Polymer-Ceramic Coating. *Mater. Technol.; Ocean Eng.* **2007**, *4*, 21–26.
- Zhang, Q.; Zhao, M.; Liu, Y.; Cao, A.; Qian, W.; Lu, Y.; Wei, F. Energy-Absorbing Hybrid Composites Based on Alternate Carbon-Nanotube and Inorganic Layers. *Adv. Mater.* **2009**, *21*, 2876–2880.
- Raney, J. R.; Fraternali, F.; Amendola, A.; Daraio, C. Modeling and *in Situ* Identification of Material Parameters for Layered Structures Based on Carbon Nanotube Arrays. *Compos. Struct.* **2011**, *93*, 3013–3018.
- Sansom, E. B.; Rinderknecht, D.; Gharib, M. Controlled Partial Embedding of Carbon Nanotubes within Flexible Transparent Layers. *Nanotechnology* **2008**, *19*, 035302–035308.
- Suhr, J.; Koratkar, N.; Keblinski, P.; Ajayan, P. M. Viscoelasticity in Carbon Nanotube Composites. *Nat. Mater.* **2005**, *4*, 134–137.
- Gama, B. A.; Bogetti, T. A.; Fink, B. K.; Yu, C.-J.; Claar, D.; Elifert, H. H.; Gillepse, J. W. Aluminum Foam Integral Armor: A New Dimension in Armor Design. *Compos. Struct.* **2001**, *52*, 381–395.
- Liu, M.; Sun, J.; Sun, Y.; Bock, C.; Chen, Q. Thickness-Dependent Mechanical Properties of Polydimethyl Siloxane Membranes. *J. Micromech. Microeng.* **2009**, *19*, 035028–035031.
- Ajayan, P. M.; Schadler, L. S.; Giannaris, C.; Rubio, A. Single-Walled Carbon Nanotube: Polymer Composites: Strength and Weakness. *Adv. Mater.* **2000**, *12*, 750–753.
- Gibson, L. J.; Ashby, M. F. *Cellular Solids: Structure & Properties*, 3rd ed.; New York, 1988; Pergamon Press.
- Barker, M. K.; Seedhom, B. B. The Relationship of the Compressive Modulus of Articular Cartilage with its Deformation Response to Cyclic Loading: Does Cartilage Optimize its Modulus so as to Minimize the Strains Arising in it Due to the Prevalent Loading Regime? *Rheumatology* **2001**, *40*, 274–284.
- Loret, B.; Simoes; Fernando, M. F. Articular Cartilage with Intra- and Extrafibrillar Waters: a Chemo-Mechanical. *Mech. Mater.* **2004**, *36*, 515–541.
- Yang, J.; Chiou, R.; Ruprecht, A.; Vicario, J.; MacPhail, A.; Rams, T. E. A New Device for Measuring Density of Jaw Bones. *Dentomaxillofacial Radiol.* **2002**, *31*, 313–316.
- Naraghi, M.; Filleter, T.; Moravsky, A.; Locascio, M.; Loutfy, R. O.; Espinosa, H. D. A Multiscale Study of High Performance Double-Walled Nanotube-Polymer Fibers. *ACS Nano* **2010**, *4*, 6463–6476.
- Zhang, M.; Atkinson, K. R.; Ray, H. Baughman. Multifunctional Carbon Nanotube Yarns by Downsizing an Ancient Technology. *Science* **2004**, *306*, 1358–1361.
- Misra, A.; Raney, J. R.; Craig, A. E.; Daraio, C. Effect of Density Variation and Non-Covalent Functionalization on the Compressive Behavior of Carbon Nanotube Arrays. *Nanotechnology* **2011**, *22*, 425705–425711.

25. Raney, J. R.; Misra, A.; Daraio, C. Tailoring the Microstructure and Mechanical Properties of Arrays of Aligned Multi-wall Carbon Nanotubes by Utilizing Different Hydrogen Concentrations during Synthesis. *Carbon* **2011**, *49*, 3631–3638.
26. Ajdari, A.; Nayeb-Hashemi, H.; Vaziri, A. Dynamic Crushing and Energy Absorption of Regular, Irregular and Functionally Graded Cellular Structures. *Int. J. Solids Struct.* **2011**, *48*, 506–516.
27. Daraio, C.; Nesterenko, V. F.; Jin, S. Highly Nonlinear Contact Interaction and Dynamic Energy Dissipation by Forest of Carbon Nanotubes. *Appl. Phys. Lett.* **2004**, *85*, 5724–5726.
28. Pushparaj, V. L.; Ci, L.; Sreekala, S.; Kumar, A.; Kesapragada, S.; Gall, D.; Nalamasu, O.; Ajayan, P. M.; Shur, J. Effects of Compressive Strains on Electrical Conductivities of a Macroscale Carbon Nanotube Block. *Appl. Phys. Lett.* **2007**, *91*, 153116–153118.
29. Shin, M. K.; Oh, J.; Lima, M.; Kozlov, M. E.; Kim, S. J.; Baughman, R. H. Elastomeric Conductive Composites Based on Carbon Nanotube Forests. *Adv. Mater.* **2010**, *22*, 2663–2667.